Environ Earth Sci (2014) 72:189–198
DOI 10.1007/s12665-013-2945-3

ORIGINAL ARTICLE

Thermo-hydro-mechanical response of granite to temperature changes

M. Najari · A. P. S. Selvadurai

Received: 1 August 2013 / Accepted: 8 November 2013 / Published online: 22 November 2013

Abstract This paper examines the thermo-hydro-mechanical behaviour of a granitic rock. The cylindrical sample of granite contained a sealed fluid-filled cavity which was subjected to a cycle of temperature changes on its outer surface. The temperature and fluid pressure changes in the fluid-filled cavity were measured. Since the measurement of fluid pressure and temperature in the sealed cavity is experimentally feasible, the technique is a common feature in thermo-hydro-mechanical experiments. However, it was observed that regardless of how precisely the cavity was filled with de-aired water, air bubbles can still exist in the cavity and influence the fluid pressure changes. A novel technique is suggested for taking into account the influence of the volume of trapped air and eliminating its effect in the estimation of permeability. The experiment was computationally modelled using the finite element code COMSOL Multiphysics^{TM} and the experimental results were compared with the computational estimates.

Keywords THM experiment · Thermo-poroelasticity · Stanstead Granite · Air entrainment · Computational modelling · Fluid-filled cavity · Thermo-poroelastic Mandel-Cryer effects

Introduction

The fully coupled theory of fluid-saturated porous media was proposed by Biot (1941) and has been widely applied to the study of problems in geomaterials where the porous skeleton either remains elastic or can experience elasto-plastic yield or continuum damage with attendant alteration in the fluid transport characteristics (Mandel 1953; Cryer 1963; Gibson et al. 1963; Rice and Cleary 1976; Mason et al. 1991; Selvadurai and Yue 1994; Yue and Selvadurai 1995; Lan and Selvadurai 1996; Mahyari and Selvadurai 1998; Selvadurai and Mahyari 1998; Wang 2000; Selvadurai 2004, 2007; Selvadurai and Shirazi 2004, 2005; Shirazi and Selvadurai 2005; Selvadurai and Ghiabi 2008; Verruijt 2013). Classical poroelasticity, however, does not take into account thermal effects. In a variety of problems such as deep geological disposal of nuclear wastes, oil and natural gas recovery and geothermal energy extraction, non-isothermal poro-mechanical modelling is essential. Biot's theory of isothermal poroelasticity was extended by a number of researchers to include non-isothermal effects (Brownell et al. 1977; Garg 1984; Booker and Savvidou 1985; Nguyen and Selvadurai 1995; Selvadurai and Nguyen 1995; Rutqvist et al. 2001; Stephansson et al. 2004; Nguyen et al. 2005; Selvadurai 2005; Wang et al. 2011; Bottcher et al. 2012; Hou et al. 2012; Selvadurai and Suvorov 2012, 2014). In this paper the coupling effects of temperature, pore pressure and skeletal deformations are investigated; the physical model was a cylindrical sample of Stanstead Granite containing a sealed fluid-filled cavity. Any fluid and heat flow within the porous medium influences the temperature and fluid pressure in the fluid-filled cavity. Since the measurement of fluid pressure and temperature in the sealed cavity is experimentally feasible, the approach was implemented in the current research. The experimental configuration was also computationally modelled, using COMSOL Multiphysics^{TM} software.

M. Najari (✉) · A. P. S. Selvadurai
Department of Civil Engineering and Applied Mechanics, McGill University, Montreal, QC, Canada
e-mail: meysam.najari@mail.mcgill.ca

Governing equations

Considering certain influences of temperature on the physical and mechanical properties of the permeating fluid, the coupled non-linear partial differential equations governing thermo-hydro-mechanical behaviour of a permeable porous geomaterial can be written in the form (Selvadurai and Nguyen 1995):

$$(K_{\mathrm{D}}+\frac{G_{\mathrm{D}}}{3})\nabla(\nabla\times\mathbf{u})+G_{\mathrm{D}}\nabla^2\mathbf{u}-\alpha\nabla p-K_{\mathrm{D}}\beta_{\mathrm{s}}\nabla T=0 \tag{1}$$

$$S\frac{\partial p}{\partial t}+\nabla\left[-\frac{K}{\mu(T)}\nabla p\right]+\alpha\frac{\partial(\nabla\times\mathbf{u})}{\partial t}-[n\beta_{\mathrm{f}}(T)+(\alpha-n)\beta_{\mathrm{s}}]\frac{\partial T}{\partial t}=0 \tag{2}$$

$$c_{\mathrm{p}}^{*}(T)\frac{\partial T}{\partial t}-k_{\mathrm{c}}^{*}\nabla^2 T=0 \tag{3}$$

These take into consideration the equation of equilibrium of the porous medium, fluid mass conservation and heat conduction in the porous medium. In Eqs. (1–3), G_{D} and K_{D} are, respectively, the shear modulus and the bulk modulus of the porous skeleton; α is the Biot coefficient and β_{s} is the volumetric thermal expansion coefficient of the solid grains; S is the specific storage of the porous skeleton; $\mu(T)$ is the dynamic viscosity of water; n is the porosity; K is permeability and β_{f} is the volumetric thermal expansion coefficient of the permeating fluid; c_{p}^{*} and k_{c}^{*} are, respectively, the specific heat capacity and thermal conductivity of the porous skeleton.

The specific storage term, S, is defined as:

$$S=nC_{\mathrm{w}}+(\alpha-n)C_{\mathrm{s}} \tag{4}$$

where C_{w} and C_{s} are, respectively, the compressibility of the pore fluid and the solid grains. Considering volume averaging, the thermal parameters are defined as:

$$k_{\mathrm{c}}^{*}=nk_{\mathrm{cf}}+(1-n)k_{\mathrm{cs}};\quad c_{\mathrm{p}}^{*}(T)=n\rho_{\mathrm{f}}(T)c_{\mathrm{f}}+(1-n)\rho_{\mathrm{s}}c_{\mathrm{s}} \tag{5}$$

where k_{cf} and k_{cs} are thermal conductivities of the liquid phase and solid phase, respectively. Also, C_{f} and C_{s} are, respectively, the specific heat capacity of the liquid phase and the solid phase.

In the modelling, the fluid-filled sealed cavity was regarded as a porous medium with a porosity of unity and a relatively high permeability (i.e. $K/K_{\mathrm{f}}=10^{-6}$) to minimize any pressure gradients and convection effects within the cavity. Also, to capture the effect of cavity volume change on the cavity pressure change, the elasticity parameters were assumed to be $v_{\mathrm{f}}=0.49$ and $E=3(1-2v_{\mathrm{f}})/C_{\mathrm{eq}}$, where C_{eq} is the compressibility of the cavity fluid that contains trapped air. The equations for modelling the fluid cavity are as follows:

$$\left(K_{\mathrm{D}}+\frac{G_{\mathrm{D}}}{3}\right)\nabla(\nabla\times\mathbf{u})+G_{\mathrm{D}}\nabla^2\mathbf{u}=0 \tag{6}$$

$$C_{\mathrm{eq}}(p)\frac{\partial p}{\partial t}+\nabla\left[-\frac{K}{\mu(T)}\nabla p\right]+\frac{\partial(\nabla\times\mathbf{u})}{\partial t}-\beta_{\mathrm{f}}(T)\frac{\partial T}{\partial t}=0 \tag{7}$$

$$\rho_{\mathrm{f}}(T)c_{\mathrm{f}}\frac{\partial T}{\partial t}-k_{\mathrm{cf}}\nabla^2 T=0 \tag{8}$$

In the above formulation, the consideration of any trapped air implies that the compressibility of the fluid in the sealed cavity is higher than the compressibility of de-aired water. A simplified relationship for the compressibility of an air–water mixture can be obtained from the Voigt bound (Christensen 1979):

$$C_{\mathrm{eq}}=\varphi C_{\mathrm{a}}+(1-\varphi)C_{\mathrm{w}} \tag{9}$$

where, φ is the air fraction in the fluid-air mixture (volume of air/volume of fluid-filled cavity), and C_{w} is the compressibility of the pure fluid, i.e. 4.54×10^{-10} Pa^{-1} (White 1986). Alternatives to Eq. (9) that take into account air solubility have also been investigated (Schuurman 1966; Fredlund 1976; Teunissen 1982; Selvadurai and Ichikawa 2013). For non-isothermal phenomena the behaviour of the air bubbles follows the ideal gas law:

$$\frac{P^{\mathrm{a}}V^{\mathrm{a}}}{T}=nR. \tag{10}$$

where V^{a} is the volume of the air, P^{a} is absolute pressure of the air bubble, T is the temperature in Kelvin, n is the number of moles and R is the universal gas constant. Considering variations in Eq. (10) we have:

$$P^{a}\mathrm{d}V^{a}+V^{a}\mathrm{d}P^{a}=nR\mathrm{d}T\Rightarrow\quad C_{\mathrm{a}}=\frac{-\frac{\mathrm{d}V^{\mathrm{a}}}{V^{\mathrm{a}}}}{\mathrm{d}P^{\mathrm{a}}}=\frac{1}{P^{\mathrm{a}}}-\frac{1}{T}\frac{\mathrm{dT}}{\mathrm{d}P^{\mathrm{a}}} \tag{11}$$

The ideal gas law also determines the changes of air fraction with pressure and temperature. Assuming that the total volume of fluids within the cavity (i.e. $V^{\mathrm{w}}+V^{\mathrm{a}}$) is constant during the THM experiment, the air fraction equation can be re-written as

$$\frac{P_0^{\mathrm{a}}V_0^{\mathrm{a}}}{T_0}=\frac{P^{\mathrm{a}}V^{\mathrm{a}}}{T};$$

$$\varphi=\frac{V^{a}}{V^{\mathrm{w}}+V^{\mathrm{a}}}\Rightarrow\varphi=\frac{\frac{P_0^{\mathrm{a}}}{P^{\mathrm{a}}}\frac{T}{T_0}V_0^{\mathrm{a}}}{V_{\mathrm{w}}+V_{\mathrm{a}}}=\frac{P_0^{\mathrm{a}}}{P^{\mathrm{a}}}\frac{T}{T_0}\varphi_0 \tag{12}$$

where P_0^{a} is the initial absolute air pressure, V_0^{a} is the initial volume of air, T_0 is the reference temperature and φ_0 is the initial air fraction in the cavity.

The other important factor in the compressibility of the air–water mixture is the dissolution of air in water. As stated by Henry's law, the weight of air that goes into solution depends on the absolute pressure of the air. Also, the rate of dissolution depends on the diffusivity rate of the air into water governed by Fick's law. The diffusivity rate for air in water is 2.0×10^{-9} m^2/s at 25 °C. The dissolved air fraction can contribute to the change in the compressibility of the air–water mixture if the rate at which air dissolves in the water is comparable to the rate at which the absolute pressure changes. Depending upon the rate of compression of an air–water mixture, the amount of air going into solution changes between 0 to $h(1-\varphi)$ of the volume of water, where h is the Henry's constant. For instance, the volume of air present in water at 25 °C can be approximately 1.78 % of the volume of water (Fredlund 1976).

Experimental investigations

The testing facility

In this paper the thermo-hydro-mechanical processes of a fluid-filled cavity in a saturated Stanstead Granite cylinder measuring 15.24 cm in diameter and 30.48 cm in height was investigated. The sample contained sealed central cavity 2.54 cm in diameter and 15.24 cm in height, which was filled with water. The outer boundary of the sample was subjected to a controlled temperature change and the temperature and pressure changes within the central fluid-filled cavity were measured. A schematic view of the test facility is shown in Fig. 1. The sample was initially vacuum saturated for 7 days and was then placed inside the water container with the central cavity facing down. An annular neoprene rubber gasket with the hardness of 60A (external diameter: 15.24 cm; internal diameter: 2.54 cm; thickness: 0.16 cm) was used to develop a seal between the plane surface of the sample and the stainless steel plate of the container. This contact area was sealed against leakage by applying a 1 MPa sealing stress to the top of the sample using a hydraulic jack. A 0.635 cm diameter hole at the center of the stainless steel plate allowed access to the central cavity. The stainless steel fitting attached to the hole was connected to a temperature-compensated pressure transducer (model: MMG150V5K4C1T4A6S; supplier: OMEGADYNE; maximum pressure: 1 MPa; accuracy: 0.2 %) to measure the cavity pressure change during the experiment. A Swagelok valve was incorporated at the stainless steel fitting to allow water inflow. Two thermocouples (type K) were placed in the top and bottom of the cavity to record the temperatures within the cavity. Following the procedure developed in previous research (Selvadurai 1996, 2002) the wires were passed through the fittings and marine epoxy was used to ensure that the connections were sealed. It should be noted that the fittings were thermally insulated using a foil-backed self adhesive foam to minimize heat loss to the ambient environment, which was maintained at approximately 25 °C. The placement of the sample inside the container was carried out under water in a large container to make sure that the central cavity was completely filled with water and with minimal air bubbles trapped within the cavity. Air can also be trapped as bubbles that stick to the inner surfaces of the fittings.

The temperature of the water surrounding the sample was controlled using two submersible heaters connected to a temperature controller unit and a thermocouple was used to measure the temperature of the water within the container. The heaters were in a configuration that allowed heating of the water around the sample without direct contact with the surface of the sample. For cooling purposes, a solenoid valve was connected to a cold water reservoir and controlled by a separate temperature controller unit and a thermocouple that measured the temperature of water inside the container. To keep an even temperature distribution in the water inside the container, the water was circulated using a fluid pump. The pump constantly extracted water from the top of the container and pumped it back into system at the lower section of the container (Fig. 1). Also, since any temperature change during the experiment can cause the sample to shrink or expand, the sealing load that was applied by the hydraulic jack could change. Thus, an accumulator with an adjustable pressure release valve was connected to the hydraulic jack to maintain the sealing load in the correct range (1 MPa $\pm$ 0.05) during the experiment. The accumulator has a piston connected to a nitrogen tank with an adjustable gas pressure regulator that maintained the load during the cooling process and a pressure release valve guaranteed that the expansion of the sample did not increase the sealing load during the heating process. It should be noted that the sealing load was measured using a load cell placed on top of the sample.

The temperature change at the cylindrical and at the top surface of the sample was measured using six thermocouples: three thermocouples measured the temperatures at the top, mid-height and bottom circumference of the sample and three thermocouples measured the temperature on the top surface of the sample (one in the center, one 2.54 cm away from the center and the third 5.08 cm away from the center). These measurements were used as temperature boundary conditions in the numerical modelling. The outer surface of the water container was covered by thermal insulation to minimize the heat loss through the Plexiglas and hence expedite the temperature increase inside the container.

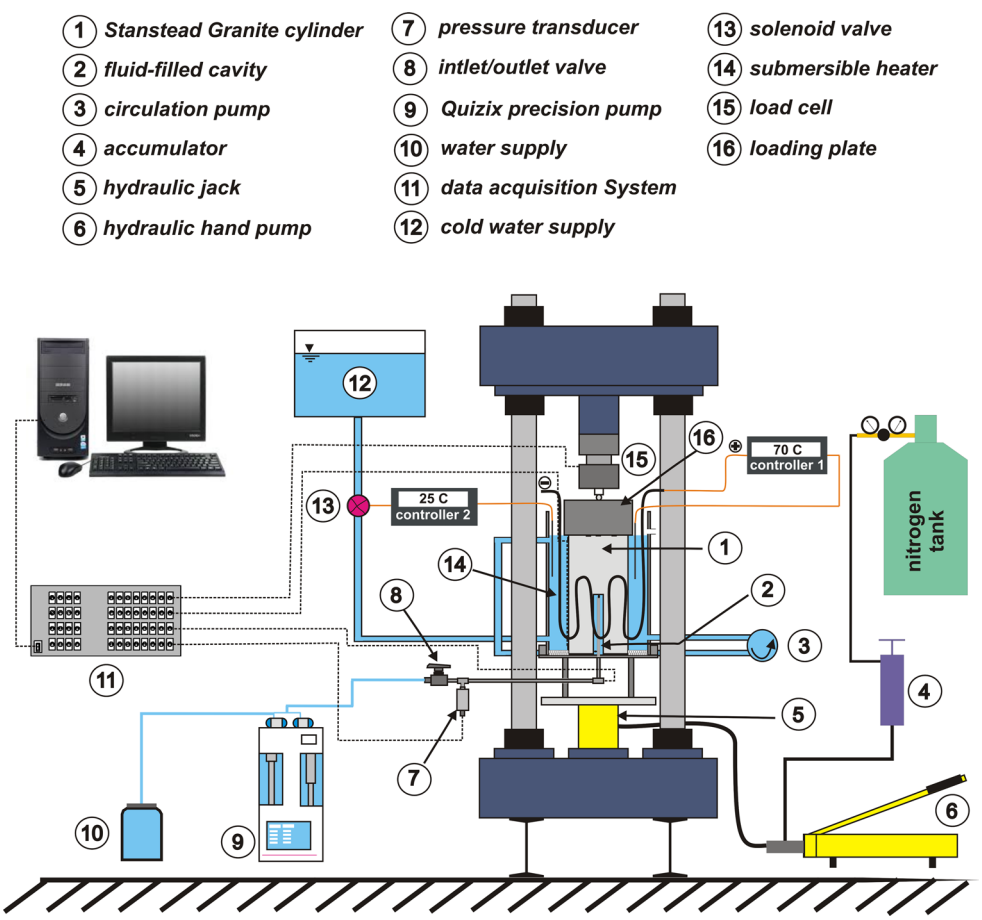

Fig. 1 Schematic view of the THM setup

Permeability measurement

Prior to performing the THM experiment, the permeability of the sample was measured using a steady state test. Three steady state tests were performed on the sample in an isothermal condition. The experiments were performed by pumping water at a constant flow rate of 0.02 ml/min using a Quizix Precision Pump (model: QX-6000; minimum flow rate, 0.00034 ml/min; accuracy of the flow rate ± 0.1 % of set flow rate; maximum pressure: 41,000 MPa). The fluid flow was continued until the cavity fluid pressure reached steady state. The results of three repeatable steady state tests were used to estimate the permeability of the Stanstead Granite sample. The COMSOL Multiphysics^{TM} finite element code was used to model the experiments. The details of validation of the COMSOL^{TM} finite element software to model hydro-mechanical phenomena are discussed by Selvadurai and Suvorov (2010, 2012) and Selvadurai et al. (2011). In these studies, the accuracy of the computational algorithms for coupled transient problems was validated through comparisons with either known or newly developed analytical solutions. The permeability of the Stanstead Granite estimated from a computational analysis of the experiments was 5.25×10^{-18} m^2. To the knowledge of the authors there are no published values for permeability of Stanstead Granite. To evaluate the efficiency of the sealing technique under high temperatures, the same steady state test was repeated under the same flow rate, while the sample was kept at 70 °C temperature. The average permeability was 5.25×10^{-18} m^2 ± 2.5 %, which validated the efficiency of the sealing technique under 70 °C temperature.

To calibrate the air–water mixture compressibility equation (i.e. Eq. (9)), the sample was first brought to a steady state condition in permeability measurement tests. The inlet valve was then closed and the decay of the cavity fluid pressure was recorded. The transient part of the experiments was used to estimate the φ_0 parameter in the compressibility equation (i.e. Eq. (9)). The results of the experiments are shown in Fig. 2. It should be noted that at the initial stage of the experiment as the cavity pressure increases from 0 to the steady state pressure value, the volume of the cavity was 116.5 ml, which included the cavity in the sample, the fittings and connections and the volume of the cylinder of the Quizix pump. In transient tests, the volume of the compressible fluid in the cavity was 98.2 ml (since the inlet valve to the cavity is closed and the volume of the cylinder of the Quizix Pump no longer contributes to the pressure changes.

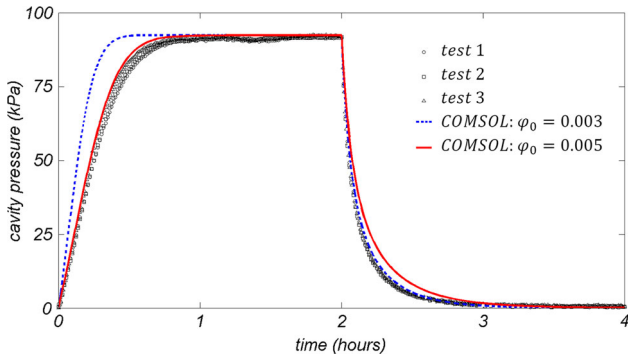

Fig. 2 Steady state tests with a flow rate of 0.02 ml/min (for 7,200 s), followed by transient decay tests

The parameters used in the COMSOL Multiphysics™ computational modelling are as follows: Young's modulus (E) = 56 GPa, Poisson's ratio (v) = 0.13; porosity (n) = 0.6 %; Biot coefficient (α) = 0.44 (Wang 2000). The transient pulse testing and the effect of the compressibility of water, the solid grains and the porous skeleton on the interpretation of permeability, are discussed in Selvadurai and Najari (2013). The bounding range of φ = (0.003–0.005) provided the best estimate for the permeability experiment, followed by a transient cavity pressure decay, as shown in Fig. 2. Since the air fraction is within the range of 0.003–0.005, the estimated air volume in the cavity would be 0.29–0.49 ml.

Thermo-hydro-mechanical experiment

Three heating–cooling cycles were carried out on the sample by changing the temperature of the water within the container. The THM test configuration is shown in Fig. 3. The temperature was initially increased from 25 °C (laboratory temperature) to 70 °C and kept constant. The heating process, including the initial temperature increase step and maintaining the constant temperature, took 4 h. The temperature on the cylindrical and plane surfaces of the sample was then reduced from 70 to 25 °C and kept constant by circulating water at 20 °C into the container. The cooling process took 8 h. The heating–cooling cycle was repeated three times and the temperature and pressure within the cavity were recorded. Each new cycle commenced after sufficient time was allowed for complete dissipation of both the temperature and pressure. Preliminary computational estimates suggest that both the pressure and temperature within the granite reduce to ambient values at approximately 12 h. The change in temperature at the cylindrical and at the upper surfaces of the sample obtained for the three cycles are shown in Fig. 4. These results were used as the temperature boundary conditions in the computational modelling.

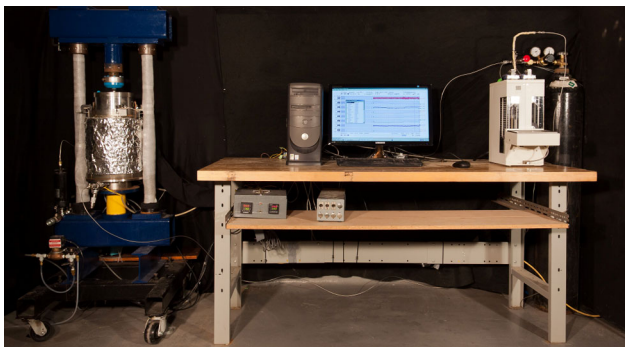

Fig. 3 Experimental configuration for performing the THM experiment

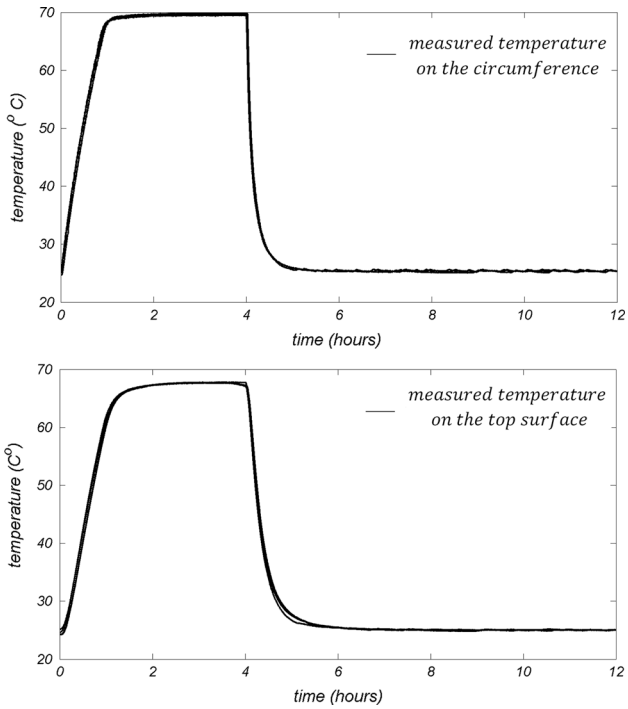

Fig. 4 The measured temperature on the cylindrical exterior surface and the upper surfaces of the sample: results of three experiments

Experimental results and computational modelling

The cavity temperature and cavity pressure measured from the three heating–cooling cycles performed on the Stanstead Granite sample are shown in Fig. 5. The trend for the change in cavity temperature is very similar to the boundary temperature change. However, there is an average time lag of 130 s between the start of the temperature change on the surface of the sample and the central cavity, resulting from the heat conduction process.

The cavity pressure initially increased due to thermal expansion of the fluid inside the cavity and from to the temperature-induced fluid flow from the porous medium towards the cavity. Note that the thermal expansion of fluid

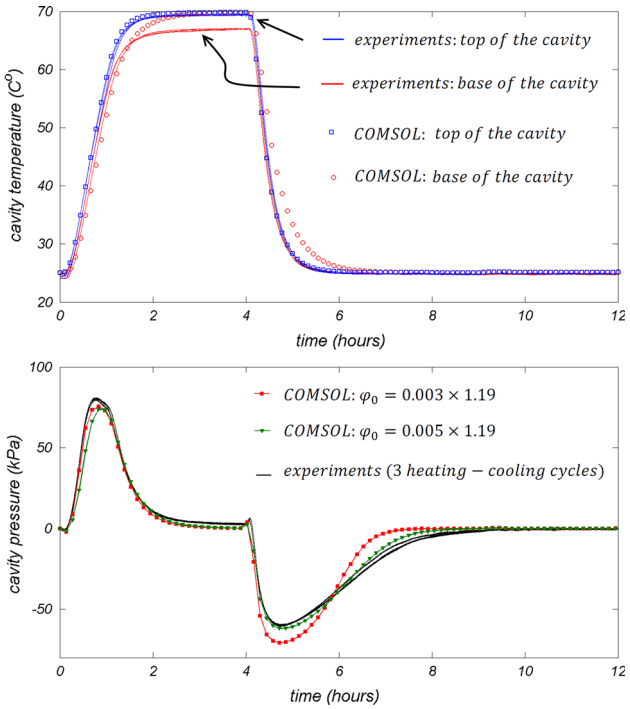

Fig. 5 The change in the cavity pressure and temperature during the three cycles of heating and cooling

within the cavity is greater than the thermal expansion of the cavity itself. The pressure in the cavity reached a maximum value of 81 kPa and then started to decay due to the dissipation of excess pore pressure through the porous medium. It can be seen that after 4 h (14,400 s) the cavity pressure reduced to zero. At this point the cooling cycle was started and the cavity pressure became negative. The minimum cavity pressure was recorded at −61 kPa. The negative pressure then started to decay over the next 8 h (28,800 s).

With respect to the rate of heating and cooling, the cooling rate in the linear range was 1.8 times faster than in the heating rate. However, the maximum cavity pressure during heating was higher than the maximum cavity pressure during cooling. This is due to the fact that, although the cavities and fittings were filled with water, there are still air bubbles entrapped in the fluid inclusion causing the compressibility of air to be pressure dependant. Based on Eq. (9), the compressibility of the air–water mixture is higher under a negative pressure than a positive pressure. Thus, the cavity pressure increase is greater during heating than in the cooling phase of the test.

The geometry and boundary conditions of the problem used in the computational modelling are shown in Fig. 6. The upper surface and the circumference of the sample had drained boundary conditions. The bottom surface, which was sealed by a rubber gasket, was modelled as a no-flow boundary condition. The temperature boundary condition for the circumference and upper surface of the sample was the temperature measured for these two surfaces; $T_1(t)$ and $T_2(t)$ are, respectively, the average temperature values measured for the three points on top, mid-height and bottom of the circumference, and center, mid-radius and the edge of the top surface of the sample. The bottom surface of the sample that was in contact with the sealing gasket was assumed to be thermally insulated. Also, the fittings and the connection tube were modelled as a stainless steel tube with an average thickness of 3 mm, which was the thickness average of the connections used. The outer surfaces of the connection tubes were thermally insulated in the experiment and thus a Neumann temperature boundary condition was assumed for that surface. A constant sealing load of 1 MPa was applied to the top surface of the sample. Since the sealing load was kept constant during the experiments, the thermo-mechanical deformation of the sample was allowed in the THM process. The parameters used in the numerical simulations are shown in Table 1. The dynamic viscosity ($\mu(T)$), volumetric thermal expansion coefficient ($\beta_f(T)$) and specific unit weight ($\rho_f(T)$) of water were assumed to be temperature dependant (Holzbecher 1998). A Lagrange-quadratic element with four degrees of freedom at each node was used in the finite element model. The displacements, pore water pressure and temperature were prescribed at all nodes. The problem contained 11,900 elements and 94,720° of freedom.

The estimated temperature changes on the top and the bottom of the cavity and the estimated cavity pressure are shown in Fig. 5. The experimental and computational results are in agreement with each other for the temperature in the top of the cavity. However, there is a slight discrepancy in the estimated temperature value in the bottom of the cavity compared to the measured value. The temperature difference at the end of the heating process is 2.45 °C. The reason for the discrepancy could be the fact that the bottom surface of the sample, which is in contact with the rubber gasket, was assumed to be thermally insulated in the computations. However, based on the experimental results obtained, there is a slight heat loss through this surface. The problem was solved using the two bounding air fraction values for the fluid cavity compressibility equation, which was obtained from the isothermal transient test presented in Sect. 3.2. The cavity pressure results agree satisfactorily with the experimental measurements. The cavity compressibility equation with $\varphi_0 = 0.003$ provided the best estimate for the positive range and the function with $\varphi_0 = 0.005$ provided the best estimate for the negative range of pressure change. A possible reason for the slight discrepancy is that the dissolution of air in water was not taken into account in the current study. Dissolution of air in water decreases the pressure in the cavity. Since in the current THM

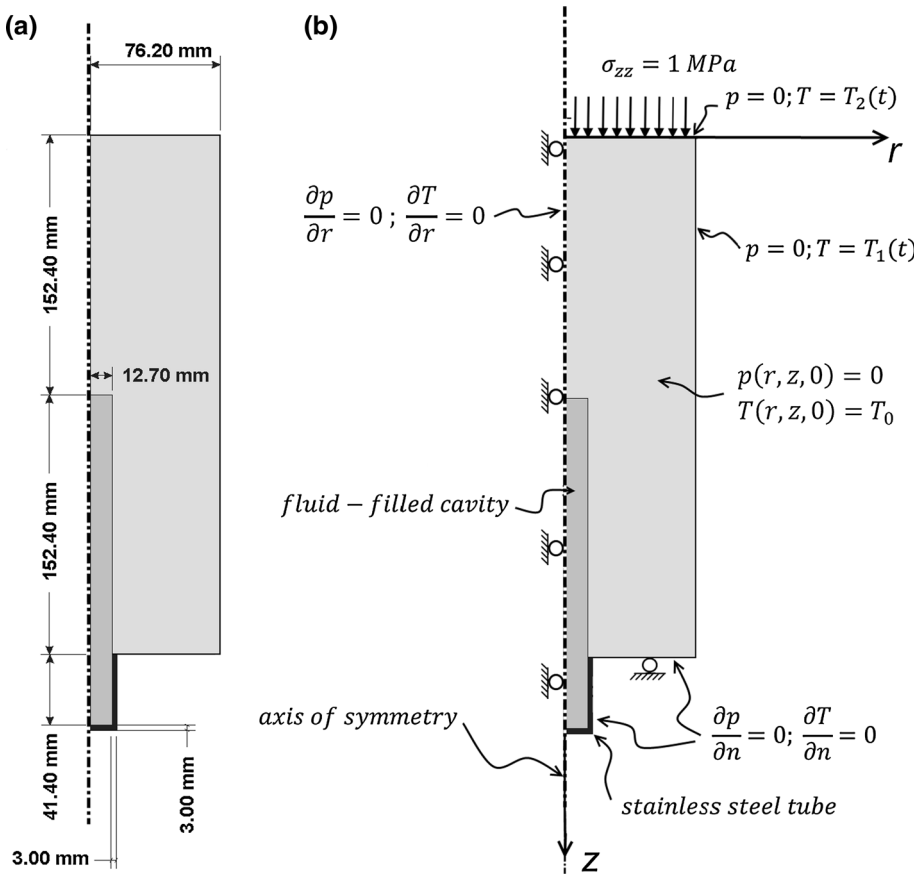

Fig. 6 Geometry and boundary conditions of the THM problem

Table 1 Values of the parameters in the computational modelling of the THM experiment

Parameter	Granite	Water	Stainless steel
Young's modulus (GPa)	56	–	200[b]
Poisson's ratio	0.13	0.49	0.3[b]
Porosity (%)	0. 6	100	–
Biot coefficient	0.44	–	–
Permeability (m^2)	5.25×10^{-18}	$(5.25 \times 10^{-18}) \times 10^6$	–
Volumetric thermal expansion coefficient ($°C^{-1}$)	3.0×10^{-5}[c]	$\beta_f(T)$[a]	4.9×10^{-5}[b]
Thermal conductivity (W m^{-1} $°C^{-1}$)	3.0[c]	0.58[a]	16.5[b]
Specific heat capacity (J kg^{-1} $°C^{-1}$)	790[c]	4187[a]	480[b]

[a] Holzbecher (1998)

[b] McGuire (2008)

[c] Nguyen et al. (2009)

experiment the pressure change in the negative range (i.e. cooling stage) is much slower than in the positive range (i.e. heating stage), there is more time for the trapped air to get partially dissolved in the water and release the pressure in the cooling stage than the heating stage. Hence, using the upper bound of the estimated air fraction better simulates the negative pressure range. Similarly, the pressure build-up stage in the isothermal permeability experiment, which was slower than the pressure decay stage, was better fitted with $\varphi_0 = 0.005$.

For the purpose of comparison the experimental results were also fitted with constant cavity fluid compressibility values. The compressibility value of $C_{eq} = 1.0 \times 10^{-8}$ Pa^{-1} provides the best estimation for the positive pressure range and the compressibility value of $C_{eq} = 1.5 \times 10^{-7}$ Pa^{-1} provides the best estimation for

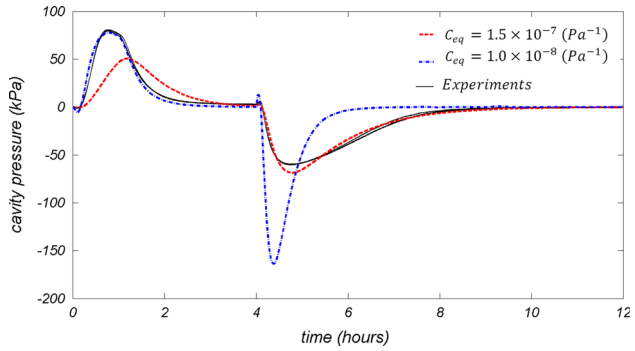

Fig. 7 Comparison of the results of THM experiments with computational results using constant compressibility values for the cavity fluid

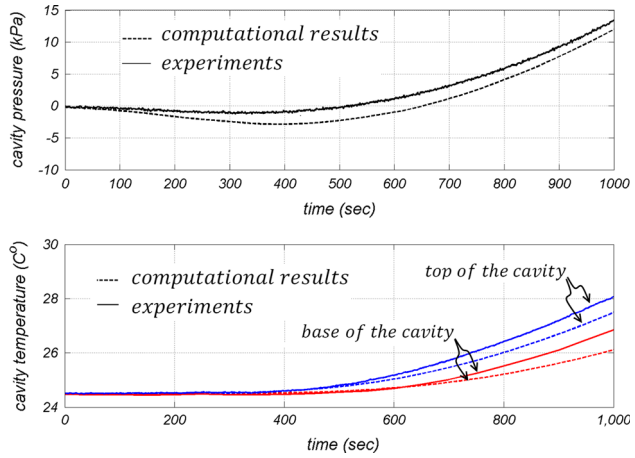

Fig. 8 Volumetric expansion of the cavity due to a temperature increase on the sample surface at the start of the heating stage ($\varphi_0 = 0.005$)

the negative pressure range. The results are shown in Fig. 7.

Another observation is that the cavity pressure changes during the early stages of heating and cooling, when the temperature change has not yet affected the cavity fluid. These effects are shown in Figs. 8 and 9. Immediately after the start of the heating stage the cavity pressure begins to decrease, reaching—1 kPa and then reducing to zero pressure after 500 s. Similarly, at the very early stage of cooling the cavity pressure increases from 2.7 kPa and reaches a maximum pressure of 6.5 kPa; it then decreases and comes back to 2.7 kPa after almost 500 s. This phenomenon is due to the fact that the very early temperature change on the surface of the sample causes the surface region of the sample to expand or shrink in heating and cooling, respectively. This is the Mandel-Cryer effect associated with temperature changes (Kodashima and Kurashige 1996; Selvadurai and Suvorov 2012).

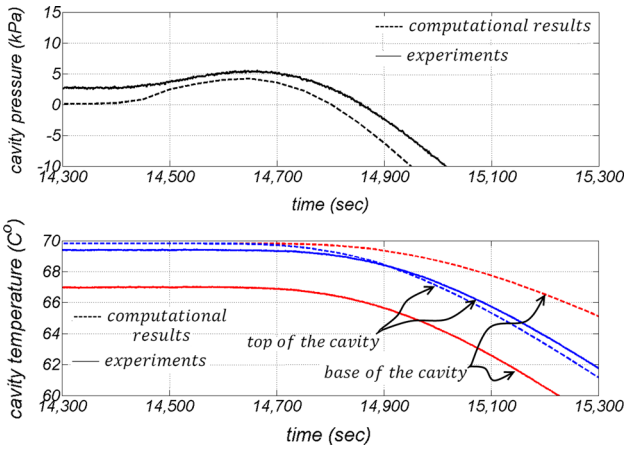

Fig. 9 Volumetric contraction of the cavity due to a temperature decrease on the sample surface at the start of the cooling stage ($\varphi_0 = 0.005$)

Conclusion

An experiment was conducted to examine the thermo-hydro-mechanical processes that can be generated in a granite cylinder with permeability in the range 5.25×10^{-18} m^2 ± 2.5 %. A fluid cavity within a cylinder is used to examine the process of pressure generation during heating of the outer surface. The experimental results were evaluated within the context of a THM model that takes into account heat conduction in the saturated granite and Darcy flow-based classical poro-elasticity. Nominal calculations were also performed to account for (1) alteration in the compressibility of the pore fluid in the system due to the presence of any air, and (2) temperature dependency in the density and fluid viscosity. The result of the experiments during heating and cooling of the cylinder indicates that pressure changes can be modelled accurately using a standard finite element software, which accommodates THM processes. The factor that contributes to the discrepancy between experimental and computational results is identified as possible air entrainment, which also accounts for the pressure-dependent compressibility. The experimentation can be further improved by adopting procedures that can minimize the influences of air content, both free and dissolved, on the THM processes. Such refinements are considered to be much too artificial since, in practice, where the theories are used to estimate the THM behaviour of rocks in situ there are no assurances of complete saturation. The research work indicates that conventional THM models can be used to model heating behaviour relatively accurately. The development of pressure within a fluid-filled cavity is the candidate problem examined to validate the modelling.

Acknowledgments The work reported in the paper was supported by NSERC Discovery and Strategic Grants awarded to A.P.S. Selvadurai.

References

Biot MA (1941) General theory of three-dimensional consolidation. J Appl Phys 12:155–164

Booker JR, Savvidou C (1985) Consolidation around a point heat source. Int J Numer Anal Meth Geomech 9:173–184

Bottcher N, Taron J, Kolditz O, Park C-H, Liedl R (2012) Evaluation of thermal equations of state for CO_2 in numerical simulations. Environ Earth Sci 67:481–495

Brownell DH, Garg SK, Pritchett JW (1977) Governing equations for geothermal reservoirs. Water Resour Res 13:929–934

Christensen RM (1979) Mechanics of composite materials. Wiley, New York

Cryer RW (1963) A comparison of three dimensional theories of Biot and Terzaghi. Q J Mech Appl Math 16:401–412

Fredlund DG (1976) Density and compressibility characteristics of air-water mixtures. Can Geotech J 13:386–396

Garg SK (1984) Formation compaction associated with thermal cooling in geothermal reservoirs. Adv Water Resour 7:188–191

Gibson RE, Knight K, Taylor PW (1963) A critical experiment to examine theories of three-dimensional consolidation. In: Proceedings of the European Conference on Soil Mechanics and Foundation Engineering, Weisbaden, vol 1, pp 69–76

Holzbecher EO (1998) Modelling density-driven flow in porous media: principles, numerics, software. Springer, Berlin

Hou Z, Gou Y, Taron J, Gorke UJ, Kolditz O (2012) Thermo-hydro-mechanical modeling of carbon dioxide injection for enhanced gas-recovery (CO_2-EGR): a benchmarking study for code comparison. Environ Earth Sci 67:549–561

Kodashima T, Kurashige M (1996) Thermal stresses in a fluid-saturated poroelastic hollow sphere. J Therm Stress 19:139–151

Lan Q, Selvadurai APS (1996) Interacting indenters on a poroelastic halfspace. J App Math Phys (ZAMP) 47:695–716

Mahyari AT, Selvadurai APS (1998) Enhanced consolidation in brittle geomaterials susceptible to damage. Mech Cohes Frict Mater 3:291–303

Mandel J (1953) Consolidation des sols (étude mathématique). Geotechnique 3:287–299

Mason DP, Solomon A, Nicolaysen LO (1991) Evolution of stress and strain during the consolidation of a fluid-saturated porous elastic sphere. J Appl Phys 70:4724–4740

McGuire MF (2008) Stainless steels for design engineers. ASM International, Chicago

Nguyen TS, Selvadurai APS (1995) Coupled thermal-mechanical-hydrological behaviour of sparsely fractured rock: implications for nuclear fuel waste disposal. Int J Rock Mech Min Sci 32:465–479

Nguyen TS, Selvadurai APS, Armand G (2005) Modelling the FEBEX THM experiment using a state surface approach. Int J Rock Mech Min Sci 42:639–651

Nguyen TS, Borgesson L, Chijimatsu M, Hernelind J, Jing L, Kobayashi A, Rutqvist J (2009) A case study on the influence of THM coupling on the near field safety of a spent fuel repository in sparsely fractured granite. Environ Geol 57:1239–1254

Rice JR, Cleary MP (1976) Some basic stress diffusion solutions for fluid-saturated elastic porous media with compressible constituents. Rev Geophys Space Phys 14:227–241

Rutqvist J, Borgesson L, Chijimatsu M, Kobayashi A, Jing L, Nguyen TS, Noorishad J, Tsang CF (2001) Thermo-hydro-mechanics of partially saturated geological media: governing equations and formulation of four finite element codes. Int J Rock Mech and Min Sci 38:105–127

Schuurman IRE (1966) The compressibility of an air-water mixture and a theoretical relation between the air and water pressures. Geotechnique 16:269–281

Selvadurai APS (1996) Heat-induced moisture movement in a clay barrier I. Experimental modelling of borehole emplacement. Eng Geol 41:239–256

Selvadurai APS (2002) Influence of pressurized water influx on the hydro-thermal behavior of an engineered clay barrier in a waste emplacement borehole. Eng Geol 64:157–178

Selvadurai APS (2004) Stationary damage modelling of poroelastic contact. Int J Solids Struct 41:2043–2064

Selvadurai APS (2005) Thermally-induced pore pressure generation in a nearly saturated cementitious material. In: Unsaturated soils: numerical and theoretical approaches, proceedings in physics, Springer 94:15–28

Selvadurai APS (2007) The analytical method in geomechanics. Appl Mech Rev 60:87

Selvadurai APS, Ghiabi H (2008) Consolidation of a soft clay composite: experimental results and computational estimates. Comput Model Eng Sci 23:53–73

Selvadurai APS, Ichikawa Y (2013) Some aspects of air-entrainment on decay rates in hydraulic pulse tests. Eng Geol 165:38–45

Selvadurai APS, Mahyari AT (1998) Computational modelling of steady crack extension in poroelastic media. Int J Solids Struct 35:4869–4885

Selvadurai APS, Najari M (2013) On the interpretation of hydraulic pulse tests on rock specimens. Adv Water Resour 53:139–149

Selvadurai APS, Nguyen TS (1995) Computational modelling of isothermal consolidation of fractured porous media. Comput Geotech 17:39–73

Selvadurai APS, Shirazi A (2004) Mandel-Cryer effects in fluid inclusions in damage susceptible poroelastic media. Comput Geotech 37:285–300

Selvadurai APS, Shirazi A (2005) An elliptical disc anchor in a damage-susceptible poroelastic medium. Int J Numer Methods Eng 16:2017–2039

Selvadurai APS, Suvorov A (2010) Application of the COMSOL multiphysics code for coupled thermo-hydro-mechanical modelling relevant to deep geologic repositories. Nuclear Waste Management Office Report NWMO TGS-509, ON, Canada

Selvadurai APS, Suvorov A (2012) Boundary heating of poroelastic and poro-elastoplastic spheres. Proc R Soc Math Phys Sci Ser A. doi:10.1098/rspa.2012.0035

Selvadurai APS, Suvorov A (2014) Thermo-poromechanics of a fluid-filled cavity in a fluid-saturated geomaterial. Proc R Soc Math Phys Sci Ser A (accepted)

Selvadurai APS, Yue ZQ (1994) On the indentation of a poroelastic layer. Int J Numer Anal Methods Geomech 18:161–175

Selvadurai APS, Suvorov A, Selvadurai PA (2011) Application of the COMSOL multiphysics code for coupled thermo-hydro-mechanical modeling of fractured rock mass subjected to glaciation loads. Nuclear Waste Management Office Report NWMO TGS-510, ON, Canada

Shirazi A, Selvadurai APS (2005) Lateral loading of a rock socket embedded in a damage-susceptible poroelastic solid. Int J Geomech 5:276–295

Stephansson O, Hudson J, Jing L (2004) Coupled thermo-hydro-mechanical-chemical processes in geo-systems; fundamentals, modelling, experiments and applications, vol 2. Elsevier, Geo-Engineering Book Series, Amsterdam

Teunissen JAM (1982) Mechanics of a fluid-gas mixture in a porous medium. Mech Mater 1:229–237

Verruijt A (2013) Theory and problems of poroelasticity. Delft University of Technology, The Netherlands

Wang H (2000) Theory of linear poroelasticity with applications to geomechanics and hydrogeology. Princeton University Press, Princeton

Wang W, Rutqvist J, Gorke U-J, Birkholzer JT, Kolditz O (2011) Non-isothermal flow in low permeable porous media: a comparison of Richards' and two-phase flow approaches. Environ Earth Sci 62:1197–1207

White FM (1986) Fluid mechanics. McGraw-Hill, New York

Yue ZQ, Selvadurai APS (1995) On the mechanics of a rigid disc inclusion embedded in a fluid saturated poroelastic medium. Int J Eng Sci 33:1633–1662